PCCP

COMMUNICATION

View Article Online
View Journal | View Issue

Cite this: *Phys. Chem. Chem. Phys.*, 2019, **21**, 2861

Received 3rd November 2018,
Accepted 9th January 2019

DOI: 10.1039/c8cp06825a

rsc.li/pccp

High hydrogen evolution activity and suppressed H_2O_2 production on Pt-skin/PtFe alloy nanocatalysts for proton exchange membrane water electrolysis†

Guoyu Shi,[a] Hiroshi Yano,[b] Donald A. Tryk,[b] Shinji Nohara[a] and Hiroyuki Uchida *[ab]

We, for the first time, demonstrate high electrocatalytic activity for the hydrogen evolution reaction (HER) on PtFe alloy nanoparticles with stabilized Pt-skin layers supported on carbon black (Pt_{xAL}–PtFe/C), which allows the reduction of Pt loading to be lowered to 1/20 compared with a conventional Pt black cathode in proton exchange membrane water electrolysis (PEMWE). The area-specific HER activity of Pt_{xAL}–PtFe/C was found to be *ca.* 2 times higher than that of commercial Pt/C at 80 °C and −0.02 V *vs.* RHE. Pt_{xAL}–PtFe/C exhibited the additional important advantage of suppressed H_2O_2 production during the HER in the presence of O_2, which inevitably diffuses from the anode in PEMWE. Both the excellent HER performance and low H_2O_2 production are attributed to the lower adsorption energies of atomic hydrogen on Pt-skin surfaces, as revealed by DFT calculations.

High purity hydrogen is produced by water electrolysis with renewable electric power (such as photovoltaics or wind power systems), which levels the output fluctuations when combined with stationary fuel cells. Proton exchange membrane water electrolyzers (PEMWEs) show advantages such as high energy conversion efficiency at high current densities, as well as a compact system with easy maintenance and start-up/shut-down. However, one of the disadvantages of conventional PEMWEs is the use of large amounts of noble metal catalysts such as (Pt + Ir) black at the oxygen-evolving anode (≥ 2 mg_{Pt+Ir} mg cm^{-2}) and Pt black at the hydrogen-evolving cathode (≥ 2 mg_{Pt} cm^{-2}).[1–6]

Our recent research has aimed to develop new electrocatalysts that can reduce the amount of noble metals down to 1/10 while maintaining high voltage efficiency ε_V exceeding 90%. We have recently succeeded in preparing new anode catalysts, IrO_x nanoparticles on doped SnO_2 supports with a fused-aggregate structure, having the potential of decreasing the Ir loading to 0.1 mg cm^{-2}, while maintaining ε_V = 90% at 1 A cm^{-2} and 80 °C.[7]

At the cathode side, Pt catalysts have been commonly used which have high activity for the hydrogen evolution reaction (HER) in acidic media. The use of Pt nanoparticles supported on carbon black (Pt/C) can reduce the Pt loading markedly, compared with Pt black,[8] but Pt black has still been predominantly employed in practical PEMWEs in order to ensure a long lifetime of the membrane-electrode assembly (MEA). During water electrolysis, O_2 generated at the anode diffuses ("crosses over") through the PEM to the cathode, resulting in the production of H_2O_2 *via* a two-electron oxygen reduction reaction (ORR), as well as possibly *via* a chemical reaction of O_2 with adsorbed H atoms (or H_2 molecules). H_2O_2 can diffuse into both the PEM and the catalyst layer. Most of the H_2O_2 can be decomposed by Pt cathode catalysts. However, OH radicals are formed in the presence of impurities such as Fe^{2+}.[9] The $HO^{\bullet}$ attacks the PEM, as evidenced by decreases in the thickness of the PEM after long-term operation.[8,10,11] It is essential to clarify whether Pt/C may intrinsically produce more H_2O_2, or it may produce more $HO^{\bullet}$ since carbon supports might take part in the radical formation.[12] Therefore, we have focused on developing highly active, highly durable catalysts for the HER with suppressed production of H_2O_2 in the presence of crossover O_2.

Recently, we have found that Pt–M (M = Fe, Co, Ni) alloy catalysts, having a stabilized Pt skin (Pt_{xAL}, one to two atomic layers), supported on carbon black (Pt_{xAL}–Pt–M/C) exhibited higher activity for the hydrogen oxidation reaction (HOR) in 0.1 M $HClO_4$ solution at 70 to 90 °C than that of commercial Pt/C (c-Pt/C). Both the kinetically-controlled area-specific activity j_k and mass activity MA_k for the HOR on the Pt_{xAL}–PtFe/C at 20 mV *vs.* reversible hydrogen electrode (RHE) were about 2 times higher than those of c-Pt/C.[13] In the present research, considering the general trend that Pt-based catalysts that display high activity for the HOR also display high activity for the HER,[14] we examine the activity for the HER on Pt_{xAL}–PtFe/C, together with clarifying the H_2O_2 formation rate during the HER in the presence of dissolved O_2, compared with those on c-Pt/C and Pt black.

[a] *Clean Energy Research Center, University of Yamanashi, Takeda 4, Kofu, 400-8510, Japan. E-mail: h-uchida@yamanashi.ac.jp*
[b] *Fuel Cell Nanomaterials Center, University of Yamanashi, Takeda 4, Kofu, 400-8510, Japan*

† Electronic supplementary information (ESI) available: Experimental details and supplementary figures. See DOI: 10.1039/c8cp06825a

The Pt_{xAL}–PtFe/C catalyst was prepared in the same manner as that described previously.[15] The specific surface area of the carbon black support was 780 $m^2\ g^{-1}$. Two commercial catalysts, c-Pt/C (46.1 mass% Pt, TEC10E50E, TKK) and Pt black (TPT-200, Tokuriki Honten Co., Ltd), were used for comparison. XRD patterns, elemental distributions, and TEM images of the catalysts are shown in Fig. S1–S3 (ESI†). Electrochemical experiments were performed using a channel flow double electrode (CFDE) cell in 0.1 M $HClO_4$ at 80 °C,[16] while the working electrode (WE) employed herein was a glassy carbon (GC) substrate in order to minimize the H_2O_2 production. The reference electrode used was a reversible hydrogen electrode (RHE), and all of the electrode potentials in this paper were given *versus* the RHE.

Fig. 1a shows iR-free polarization curves for the HER on Pt_{xAL}–PtFe/C, c-Pt/C, and Pt black in H_2-saturated 0.1 M $HClO_4$ at 80 °C, in which the current is shown as the apparent mass activity (MA). The value of MA at all potentials increased in the order Pt black < c-Pt/C < Pt_{xAL}–PtFe/C. The apparent area-specific activities (j_s, based on the electrochemically active area, ECA) at −0.02 V on these catalysts are shown in Fig. 1b. Since the value of j_s on c-Pt/C is comparable to that of Pt black, the higher MA on c-Pt/C than that of Pt black is well explained by its larger ECA (69.7 $m^2\ g_{Pt}^{-1}$ *vs.* 6.8 $m^2\ g_{Pt}^{-1}$). Notably, the value of j_s on Pt_{xAL}–PtFe/C was about 2 times higher than that of c-Pt/C, providing high MA, *e.g.*, the MA of Pt_{xAL}–PtFe/C at −0.02 V was −1.62 A mg_{Pt}^{-1}, which is about 1.6 times higher and 20 times higher than that of c-Pt/C (−1.01 A mg_{Pt}^{-1}) and Pt black (−0.08 A mg_{Pt}^{-1}), respectively. In addition, an accelerated durability test of the catalysts was conducted by potential cycling between −0.03 and 0.95 V at 80 °C in N_2-purged 0.1 M $HClO_4$, which simulates the start–stop cycles for PEMWEs (see Fig. S4, ESI†). As shown in Fig. 2, the HER MA loss of Pt_{xAL}–PtFe/C at −0.03 V after 5000 cycles was only 8%, whereas c-Pt/C showed a larger loss of 20%. The increased durability of Pt_{xAL}–PtFe/C was attributed to the uniform particle size of Pt_{xAL}–PtFe, as well as the increased rigidity of the Pt skin/alloy structure.[13,17] Such superior properties (HER activity and durability) of Pt_{xAL}–PtFe/C at the practical operating temperature would make it possible to reduce the Pt loading for the PEMWE.

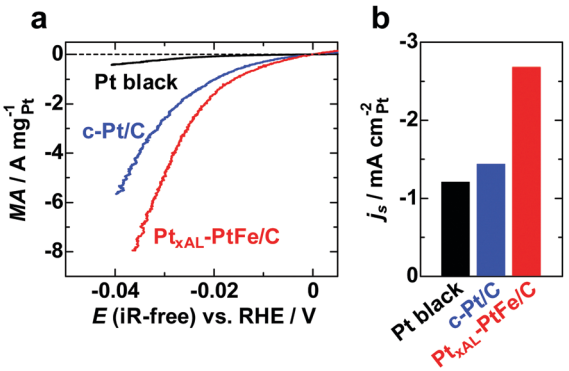

Fig. 1 (a) HER polarization curves (iR-free) of Nafion-coated electrodes in H_2-saturated 0.1 M $HClO_4$ (mean flow rate of 111 cm s^{-1}) at 80 °C with potential scan rate of 5 mV s^{-1}, and (b) apparent Pt area-specific activity (j_s) at −0.02 V *vs.* RHE.

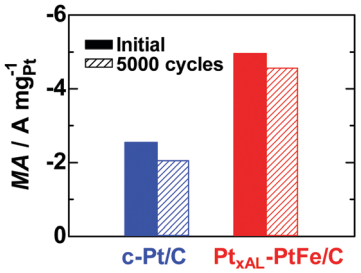

Fig. 2 Changes in MA values for the HER at −0.03 V and 80 °C measured after 5000 potential cycles (hatched bars) between −0.03 and 0.95 V in N_2-purged 0.1 M $HClO_4$ with the scan rate of 0.1 V s^{-1} (see Fig. S4, ESI†).

Next, we have measured the H_2O_2 production rates at these catalysts during the HER. H_2O_2 emitted from the WE of the CFDE was detected as the oxidation currents at the collecting electrode (CE) while hydrogen was also being generated at the WE. We note that the H_2 generated at the WE would also, in principle, be detected as HOR current at the CE, but, at the high potential (1.4 V) of the CE, the HOR is experimentally found to be suppressed.[18] Raw data are shown in Fig. S5 (ESI†). In any case, the small background current is subtracted. Fig. 3 shows the potential dependence of the H_2O_2 oxidation current density at the CE (a measure of H_2O_2 production rate, $r(H_2O_2)$ at the three catalysts during the HER) measured in O_2-saturated 0.1 M $HClO_4$ solution. A general trend for all catalysts is that the $r(H_2O_2)$ increases gradually from 0 to *ca.* −0.06 V. The $r(H_2O_2)$ on Pt black was nearly identical with that of Pt/C between 0 to −0.03 V, but it became lower at increasingly negative potentials, which may be the reason for the use of Pt black so far. The $r(H_2O_2)$ on Pt_{xAL}–PtFe/C was clearly lower than those on Pt black or Pt/C. Below −0.06 V, the $r(H_2O_2)$ steeply decreased for Pt black and Pt/C. Such trend was also seen for Pt_{xAL}–PtFe/C, but the peak potential shifted negatively (−0.07 V). The H_2O_2 yields $P(H_2O_2)$, *i.e.*, the percentage of H_2O_2 production *versus* the total current at the WE, are also shown in Fig. S6 (ESI†). The values of $P(H_2O_2)$ on these catalysts decreased monotonically with decreasing potential. Pt_{xAL}–PtFe/C exhibited substantially lower $r(H_2O_2)$ than those of Pt black and Pt/C, especially in the potential range from 0 to −0.06 V. The suppression of H_2O_2 production at the cathode, as seen for the lower values of $P(H_2O_2)$ and $r(H_2O_2)$, can contribute with certainty to mitigating the chemical degradation of membranes or MEAs.

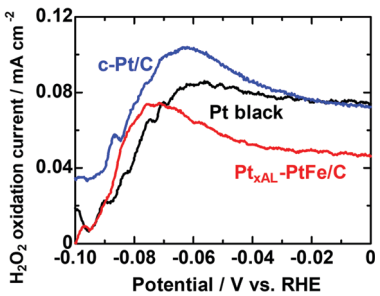

Fig. 3 Potential-dependent H_2O_2 oxidation current density for various catalysts measured in O_2-saturated 0.1 M $HClO_4$ solution at 80 °C.

Here, we propose that both the increase and decrease of $r(H_2O_2)$ are due to reactions involving adsorbed hydrogen, specifically, involving O_2 to produce H_2O_2, and, in turn, its further reduction. It is well known for Pt single crystal electrodes that H_2O_2 can be produced quantitatively on the Pt(111) surface in the low-potential region where the coverage of underpotentially deposited hydrogen atoms $\theta(H_{UPD})$ is high.[19] This effect also can operate with Pt/C catalysts.[20,21] Thus, H_2O_2 is produced predominantly on (111) facets of the Pt nanoparticles due to end-on adsorption of O_2, with the neighboring sites blocked by H_{UPD}. It has been clarified that the adsorption of H_{UPD} on the (111) face of Pt–Ni or Pt–Co alloy is weaker and the $\theta(H_{UPD})$ is lower than that of Pt(111).[22,23] From the cyclic voltammograms for the three catalysts in N_2-saturated solution (Fig. S7, ESI†), it is clear that the H_{UPD} adsorption on Pt_{xAL}–PtFe/C is shifted toward less positive potentials, suggesting that the surface sites for O_2 adsorption would be less blocked by H_{UPD}, reducing the end-on adsorption of O_2 and subsequent H_2O_2 production.

In order to understand the details of the increased rate for the HER and suppressed rate of H_2O_2 production on Pt skin–PtFe/C, density functional theory (DFT) calculations were carried out based on the stepped (221) surface, which includes (110) steps and (111) terraces, similar to those adopted in our previous work.[13] In the present work, we consider that the steps are active sites for the coupled association of hydrogen atoms and desorption of H_2, commonly referred to as the Tafel step, as described by Santana *et al.* in their DFT study of the HOR and HER on Pt(110).[24] As shown in Table 1, the H adsorption energy at the (110) step edge of Pt skin/PtFe(221) is smaller than that of Pt(221). The activation energy for the Tafel step calculated is closely related to the H adsorption energy: Pt skin/PtFe(221) exhibited a smaller activation energy by 0.42 eV, compared with Pt(221) (see Fig. S8, ESI†). Thus, the higher rate for the HER on Pt_{xAL}–PtFe/C is reasonably explained by the decreased H adsorption energy.

Interestingly, on the (111) terraces of Pt skin/PtFe(221), the H adsorption energy was found to be even more significantly decreased, being smaller by 0.83 eV than that for Pt(221). This is consistent with lower $\theta(H_{UPD})$ on the Pt skin/PtFe than those of Pt/C or Pt black, as shown in Fig. S7 (ESI†). In order to calculate the adsorption energy of H_{UPD} as a function of coverage, we have used flat (111) models. As shown in Fig. S9 (ESI†), a honeycomb structure of the bridging H could be simulated at potentials below 0 V.[25,26] As summarized in Table 2, the adsorption energies are similar to those for the (111) terraces on the (221) surfaces (see Table 1), especially for Pt(111). Irrespective of $\theta(H_{UPD})$, Pt skin/PtFe(111) showed significantly lowered H adsorption energies than those for Pt(111).

Table 1 Adsorption energies (eV) of 2H and O_2 on Pt(221) and Pt skin/PtFe(221) surfaces

Adsorption site	Pt(221)	Pt skin/PtFe(221)
(110) step edge-2H	−1.37	−0.94
(110) step edge-O_2	−1.71	−1.10
(111) terrace-2H	−0.91	−0.08

Table 2 Adsorption energies (eV) of H on Pt(111) and Pt skin/PtFe(111) surfaces at $\theta(H_{UPD})$ = 1/9, 1 and $\theta(H_{UPD})$ + $\theta(H_{OPD})$ = 4/3

$\theta(H_{UPD})$	Pt(111)	Pt skin/PtFe(111)
1/9	−1.05	−0.38
1	−0.99	−0.36
4/3	−0.86	−0.17

It is also important to discuss the role of the overpotentially deposited hydrogen H_{OPD} in these reactions. The H_{OPD} has been proposed to form below 0.1 V and to be involved in the HER. However, it differs from the H adsorbed at (110) steps discussed above, which is associated with a CV peak often observed at *ca.* 0.1 V.[27] Specifically, we have reported that an intermediate of the HER on Pt is atomic H in the atop configuration, based on the *in situ* FTIR study, *i.e.*, a peak of 2080–2090 cm^{-1} observed at potentials less positive than *ca.* 0.1 V was assigned to the H_{OPD} on a polycrystalline Pt film electrode.[28] Such an assignment has been validated by DFT studies on Pt(111).[25,26] The adsorption energies of the H_{OPD} are smaller than those of H_{UPD}, resulting in lower average adsorption energy (Table 2 and Fig. S10, ESI†). The very weak adsorption of H means that, after its formation, it is very reactive, as discussed below.

The H_{OPD} could chemically reduce O_2 to form H_2O_2 (step 1 in Fig. S11, ESI†), and subsequently reduce H_2O_2 further to H_2O (step 2 in Fig. S8 and S11, ESI†). The gradual increase of $r(H_2O_2)$ at potentials between 0 to −0.06 V, and rapid decreases in $r(H_2O_2)$ at less positive potentials on all three catalysts (Fig. 3) can be explained well by the stepwise reduction of O_2, based on our FTIR result that the coverage of H_{OPD} increases gradually below 0.1 V and increases steeply with further increase in the cathodic overpotential.[28] Thus far, we have explained the potential-dependence of H_2O_2 formation shown in Fig. 3. Further, the DFT calculations suggests a more facile reduction of H_2O_2 with H_{OPD} on Pt skin/PtFe(111) in comparison with Pt(111) (Fig. S12, ESI†), by 0.8 eV more exothermic, which can delay or slower the formation of H_2O_2, as seen for the less positive peak potential in Fig. 3. Thus, based on both indirect experimental and DFT results, we conclude that the weaker adsorption of both H_{UPD} and H_{OPD}, affording reduced end-on adsorption of O_2, as well as easier H_2O_2 reduction by H_{OPD} on the Pt_{xAL}–PtFe surface, is responsible for the smaller H_2O_2 production rate. However, obtaining direct experimental evidence addressing this point is challenging and will be the subject of ongoing research.

In addition, it was found that the HER rates on all catalysts were suppressed by the presence of O_2 (Fig. S5, ESI†). The suppression was comparable for Pt_{xAL}–PtFe/C and c-Pt/C (by 13%) and somewhat larger for Pt black (by 20%) at −0.1 V in 0.1 M $HClO_4$ solution saturated with O_2 (1 atm). This is consistent with the strong adsorption of O_2 at the HER-active step sites (Table 1). However, such a high O_2 concentration would not normally exist at the cathode catalyst layer/PEM interface, and thus, the depression of the HER current would be much lower. In any case, it is necessary to examine the actual oxygen concentration in the operating cell and its effects.

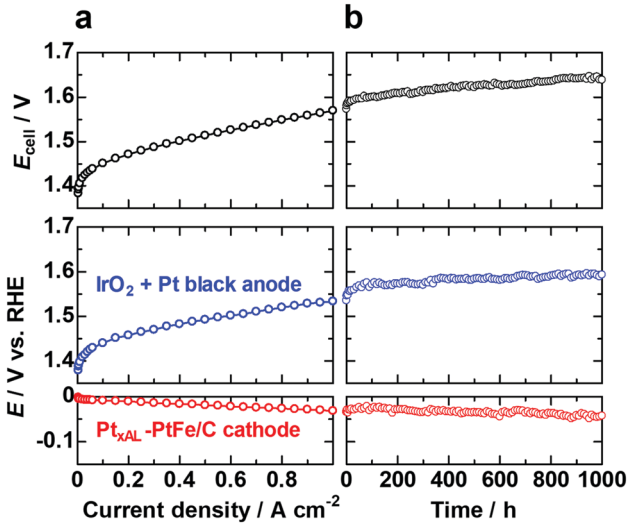

Fig. 4 (a) Polarization curves for PEMWE single cell with Pt_{xAL}–PtFe/C cathode (0.2 mg_{Pt} cm^{-2}) and IrO_2 + Pt black anode (0.92 mg_{Ir+Pt} cm^{-2}) at 80 °C showing cell potential, anode potential and cathode potential from top to bottom. The electrolyte membrane was NRE212 (50 μm thick). (b) Potential variations during the long-term cell test at 1 A cm^{-2} and 80 °C.

We have also examined the performance and durability of the Pt_{xAL}–PtFe/C cathode catalyst (0.2 mg_{Pt} cm^{-2}, 1/10 that of standard Pt black) and a conventional anode (IrO_2 + Pt black) in a PEMWE single cell with a reference electrode (RHE). The polarization curves recorded for cell potential and the electrode potentials *vs.* RHE are shown in Fig. 4a. The cell potential E_{cell} was 1.57 V (voltage efficiency of 94.3%) at 1 A cm^{-2} and 80 °C. The Pt_{xAL}–PtFe/C cathode was found to operate stably for continuous operation at 1 A cm^{-2} and 80 °C for 1000 h (Fig. 4b). In particular, we found that the membrane thickness was virtually unchanged (about 50 μm) after the durability test for 1000 h (Fig. S13, ESI†), suggesting that the formation of H_2O_2 near the Pt skin–PtFe/C cathode was possibly suppressed, which would be consistent with the CFDE results presented above. To further confirm that decreased H_2O_2 production results in increased cell stability, a cell stability test with a cathode consisting of a commercial Pt/C catalyst will be carried out and reported elsewhere.

In conclusion, we report herein a new hydrogen evolution electrocatalyst having a Pt-skin surface on PtFe alloy nanoparticles dispersed on a carbon support (Pt_{xAL}–PtFe/C). It exhibited *ca.* 2-times higher HER specific activity than commercial Pt catalysts, together with lower H_2O_2 production during the HER in the presence of O_2. DFT results suggest that weak H adsorption on the Pt skin/PtFe surface boosts the HER while suppressing H_2O_2 production. This work contributes to expanding the understanding of HER electrocatalysis with accompanying H_2O_2 formation, as well as the cost reduction of PEM electrolysis devices, which should promote larger scale application.

Conflicts of interest

There are no conflicts to declare.

Acknowledgements

This work was supported by "Fundamental Research on Highly Efficient Polymer Electrolyte Water Electrolyzers with Low Noble Metal Electrocatalysts" from Grant-in-Aid No. 17H01229 for Scientific Research (A) from the Japan Society for the Promotion of Science.

Notes and references

1 A. Jain and A. Ramasubramaniam, *Phys. Chem. Chem. Phys.*, 2018, **20**, 23262–23271.
2 K. Ojha, S. Saha, P. Dagar and A. K. Ganguli, *Phys. Chem. Chem. Phys.*, 2018, **20**, 6777–6799.
3 G. Zhang, K. Ming, J. Kang, Q. Huang, Z. Zhang, X. Zheng and X. Bi, *Electrochim. Acta*, 2018, **279**, 19–23.
4 Q. Feng, G. Liu, B. Wei, Z. Zhang, H. Li and H. Wang, *J. Power Sources*, 2017, **366**, 33–55.
5 M. Carmo, D. L. Fritz, J. Mergel and D. Stolten, *Int. J. Hydrogen Energy*, 2013, **38**, 4901–4934.
6 M. K. Debe, S. M. Hendricks, G. D. Vernstrom, M. Meyers, M. Brostrom, M. Stephens, Q. Chan, J. Willey, M. Hamden, C. K. Mittelsteadt, C. B. Capuano, K. E. Ayers and E. B. Anderson, *J. Electrochem. Soc.*, 2012, **159**, K165–K176.
7 H. Ohno, S. Nohara, K. Kakinuma, M. Uchida, A. Miyake, S. Deki and H. Uchida, *J. Electrochem. Soc.*, 2017, **164**, F944–F947.
8 S. A. Grigoriev, K. A. Dzhus, D. G. Bessarabov and P. Millet, *Int. J. Hydrogen Energy*, 2014, **39**, 20440–20446.
9 M. Aoki, H. Uchida and M. Watanabe, *Electrochem. Commun.*, 2006, **8**, 1509–1513.
10 M. Chandesris, V. Médeau, N. Guillet, S. Chelghoum, D. Thoby and F. Fouda-Onana, *Int. J. Hydrogen Energy*, 2015, **40**, 1353–1366.
11 F. Fouda-Onana, M. Chandesris, V. Médeau, S. Chelghoum, D. Thoby and N. Guillet, *Int. J. Hydrogen Energy*, 2016, **41**, 16627–16636.
12 E. Endoh, S. Terazono and H. Widjaja, *Electrochem. Solid-State Lett.*, 2004, **7**, A209–A211.
13 G. Shi, H. Yano, D. A. Tryk, A. Iiyama and H. Uchida, *ACS Catal.*, 2016, **7**, 267–274.
14 N. M. Marković, B. N. Grgur and P. N. Ross, *J. Phys. Chem. B*, 1997, **101**, 5405–5413.
15 M. Watanabe, H. Yano, D. A. Tryk and H. Uchida, *J. Electrochem. Soc.*, 2016, **163**, F455–F463.
16 H. Yano, E. Higuch, H. Uchida and M. Watanabe, *J. Phys. Chem. B*, 2006, **110**, 16544–16549.
17 G. Shi, H. Yano, D. A. Tryk, M. Matsumoto, H. Tanida, M. Arao, H. Imai, J. Inukai, A. Iiyama and H. Uchida, *Catal. Sci. Technol.*, 2017, **7**, 6124–6131.
18 C. M. Zalitis, J. Sharman, E. Wright and A. R. Kucernak, *Electrochim. Acta*, 2015, **176**, 763–776.
19 N. Markovic, H. Gasteiger and P. N. Ross, *J. Electrochem. Soc.*, 1997, **144**, 1591–1597.
20 M. Neergat, V. Gunasekar and R. K. Singh, *J. Electrochem. Soc.*, 2011, **158**, B1060–B1066.

21 M. Inaba, H. Yamada, J. Tokunaga and A. Tasaka, *Electrochem. Solid-State Lett.*, 2004, **7**, A474–A476.
22 V. R. Stamenkovic, B. Fowler, B. S. Mun, G. F. Wang, P. N. Ross, A. Lucas and N. M. Markovic, *Science*, 2007, **315**, 493.
23 M. Wakisaka, S. Morishima, Y. Hyuga, H. Uchida and M. Watanabe, *Electrochem. Commun.*, 2012, **18**, 55–57.
24 J. A. Santana, J. J. Mateo and Y. Ishikawa, *J. Phys. Chem. C*, 2010, **114**, 4995–5002.
25 J. J. Mateo, D. A. Tryk, C. R. Cabrera and Y. Ishikawa, *Mol. Simul.*, 2008, **34**, 1065–1072.
26 Y. Ishikawa, J. J. Mateo, D. A. Tryk and C. R. Cabrera, *J. Electroanal. Chem.*, 2007, **607**, 37–46.
27 Q. S. Chen, F. J. Vidal-Iglesias, J. Solla-Gullon, S. G. Sun and J. M. Feliu, *Chem. Sci.*, 2012, **3**, 136–147.
28 K. Kunimatsu, H. Uchida, M. Osawa and M. Watanabe, *J. Electroanal. Chem.*, 2006, **587**, 299–307.